# Design and Experimental Verification of an Equivalent Forebody Representation of Flowing Inlets

Davy A. Haynes* and David S. Miller*
*NASA Langley Research Center, Hampton, Virginia*
and
John R. Klein† and Check M. Louie†
*McDonnell Aircraft Company, St. Louis, Missouri*

**A method by which a simple equivalent-faired body can be designed to replace a more complex body with flowing inlets has been demonstrated for supersonic flow. An analytically defined, geometrically simple faired inlet forebody has been designed using a linear potential code to generate flow perturbations equivalent to those produced by a much more complex forebody with inlets. An equivalent forebody wind-tunnel model was fabricated, and a test was conducted in NASA Langley Research Center's Unitary Plan Wind Tunnel. The test Mach number range was 1.6–2.16 for angles of attack of −4–16 deg. Test results show that, for the purposes considered here, the equivalent forebody simulates the original flowfield disturbances to an acceptable degree of accuracy.**

## Nomenclature

| | | |
|---|---|---|
| $a$ | = | elliptical section, semimajor axis |
| $b$ | = | model wing span, 17.27 in. |
| $b_u$ | = | upper semi-ellipse, semiminor axis |
| $b_l$ | = | lower semi-ellipse, semiminor axis |
| $C_D$ | = | drag coefficient |
| $C_{Df}$ | = | skin-friction drag coefficient |
| $C_L$ | = | lift coefficient |
| $C_m$ | = | moment coefficient |
| $c$ | = | wing local chord |
| $\bar{c}$ | = | wing mean aerodynamic chord, 14.33 in. |
| $M_R$ | = | model moment resolving center, 18.93 in. aft of nose |
| $S$ | = | model reference area, 200.75 in.$^2$ |
| $u,v,w$ | = | Cartesian perturbation velocity components |
| $x,y,z$ | = | Cartesian coordinates |
| $\epsilon$ | = | exponent of the superelliptic sections |

## Introduction

In the arena of supersonic aerodynamics, both computational and experimental research can be expensive in terms of computational computer time, experimental model fabrication, and wind-tunnel operation costs. As part of an ongoing cooperative wing-design study by the Supersonic/Hypersonic Aerodynamics Branch of the NASA Langley Research Center and the McDonnell Aircraft Company, an effort was undertaken to develop a method by which a complex forebody of a generic supercruise fighter could be replaced with a much simpler equivalent-faired forebody. The ability to design such an equivalent-faired forebody would significantly reduce computational numerical model complexity as well as model fabrication costs. This equivalent forebody concept for supersonic speeds was an outgrowth of a similar method that has been successfully applied at transonic speeds.[1]

This supersonic application and experimental validation of the concept was conducted on the Air Force Wright Aeronautical Laboratory generic fighter wind tunnel model (Fig. 1). The original forebody features a drooped nose with canopy and twin side-mounted flowing inlets with boundary-layer diverters separating the inlets from the fuselage. The inlets and boundary-layer diverters represent geometric complexities not amenable to the modeling capabilities of most Euler and Navier-Stokes computational methods. Thus, the equivalent forebody approach is a means of eliminating the discontinuities caused by the inlets and boundary-layer diverters, thereby bypassing numerical modeling restrictions while still considering the overall influence of the fuselage for wing design purposes. In many cases, this approach allows the use of an analytical description of the forebody in computational models, and it eliminates the expensive and complicated design and fabrication of model inlets with internal full-flowing ducts and exit choke rings.

The equivalent forebody was required to duplicate the disturbances of the original complex forebody on the wing flowfield at a design point of Mach 1.8 and $C_L$ of 0.3. Specifically, an equivalent forebody was sought to duplicate the original forebody/inlet velocity perturbations on the wing flowfield. Additionally, geometric constraints were imposed on the

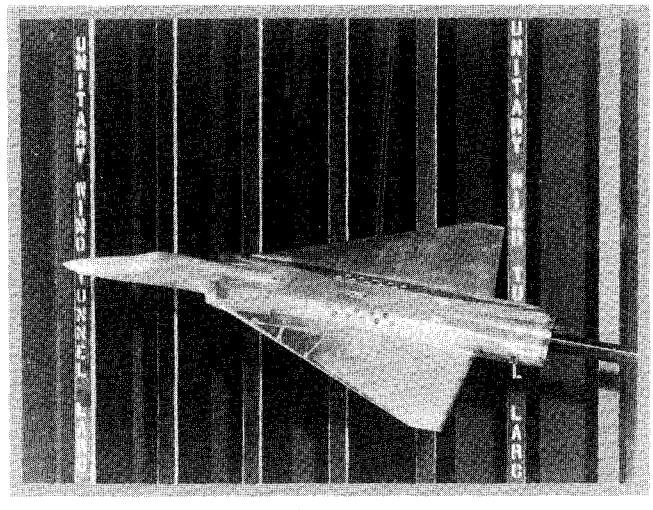

**Fig. 1 Original configuration installation photograph.**

Presented as Paper 88-0195 at the AIAA 26th Aerospace Sciences Meeting, Reno, NV, Jan 11–14, 1988; received Feb. 5, 1988; revision received Dec. 24, 1988. 

*Aerospace Engineer, Supersonic/Hypersonic Aerodynamics Branch. Member AIAA.
†Engineer, Aerodynamics. Member AIAA.

equivalent forebody design, and will be discussed in a subsequent section. To validate the concept, an equivalent forebody was designed for the existing generic supersonic wind-tunnel model and tested in NASA Langley's Unitary Plan Wind Tunnel. The test Mach number range was 1.6–2.16 with angles of attack up to 16 deg. Surface pressures, forces, and moments were measured and flow-visualization photographs were taken for both the original and equivalent configurations.

## Discussion

The PAN AIR linear-theory panel method[2] was chosen to compute the flowfields about a three-dimensional model of the original configuration, as shown in Fig. 2. Thus, nonlinear and viscous effects were not considered in the design of the equivalent forebody. Arbitrary vertical and horizontal survey planes were employed in the PAN AIR models to obtain the flowfield perturbation velocities due to the forebody. The design conditions were Mach 1.8 and a $C_L$ of 0.3, which correspond to a maneuver flight condition at approximately 9 deg angle of attack. Then, as shown in Fig. 2, the original forebody was replaced with a smooth, analytically defined forebody, and PAN AIR was used iteratively on geometric variations of this forebody. The goal was to match as closely as possible the longitudinal, lateral, and vertical velocity perturbations of the original forebody in selected survey planes. Meanline camber and the distributions of normal cross-sectional area, maximum breadth and upper and lower thickness were each varied in the iterative process.

A notable characteristic of the original wind-tunnel model crucial to the success of this approach is that, at Mach 1.8, the inlets operate in a near-critical condition. Mass flow ratio for the inlets has been experimentally determined[3] to be 0.95. Shadowgraphs confirm that any effects of normal shocks are confined to the internal ducts limiting external, nonisentropic compression to that produced by the oblique shock emanating from the inlet lip. This experimental evidence of weak, external compression adds confidence to the assumption that a panel method, with its small disturbance assumption, would be acceptable for such a task.

Because the equivalent forebody was to be a retrofit to an existing wind-tunnel model, geometric design constraints were required. The contour of the equivalent forebody was constrained to match that of the center fuselage at the forebody/center fuselage splice station. Additionally, the width of the equivalent forebody aft of the wing/fuselage junction was constrained by the existing wing set. The models in Fig. 2 illustrate that portion of the fuselage to be replaced.

### Equivalent Forebody Design

In the first step of the equivalent forebody design the PAN AIR code was used to determine the flowfield about the original forebody. The original forebody was then replaced with an analytically defined forebody. Since the fuselage cross section at the splice station resembled an ellipse with the major axis in the horizontal plane, the faired-inlet forebody was initially defined as elliptical cross sections. A forebody camber line established the locus of the elliptical cross sections. The equivalent forebody sections were defined by upper and lower semi-ellipses using different upper and lower semiminor axes. A diagram of the equivalent forebody geometry definition is shown in Fig. 3.

Initial PAN AIR surveys of the perturbation velocities of the original forebody were conducted for three survey plane stations. The locations were in the wing $xy$ plane at 1, 3, and 5 % of the wing local chord ahead of the wing leading edge. There was generally little spanwise variation in the perturbation components between the three survey plane locations. Therefore, the survey planes located at the 3% station (ahead of the wing local chord) were selected for all subsequent analyses.

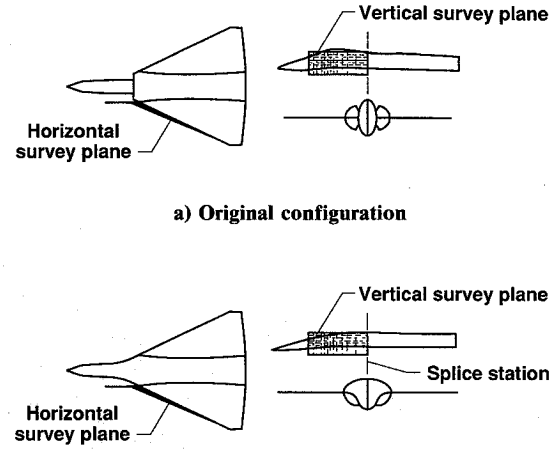


Fig. 2 PAN AIR computational models.

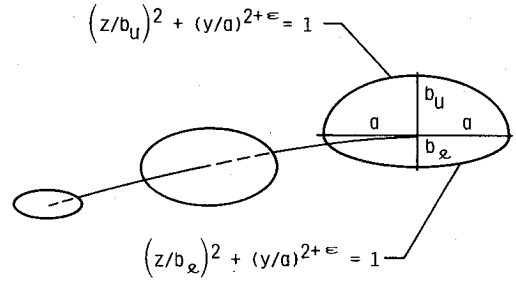


Fig. 3 Equivalent forebody analytical definition.

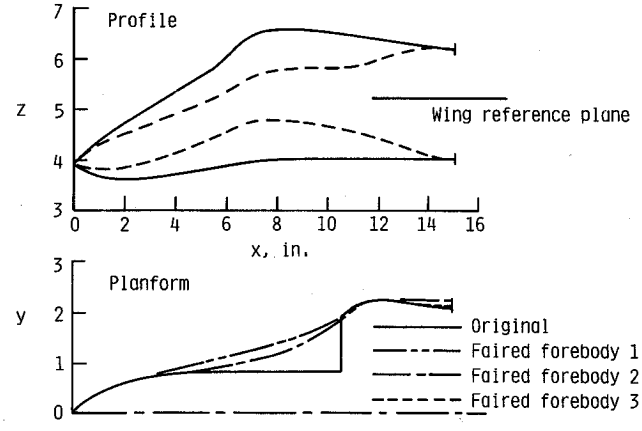


Fig. 4 Profile and planform comparison.

The geometries of the first two faired-forebody iterations were patterned after the original forebody camber and profile. This fixed the camber line as well as the upper and lower semiminor axes. The major axis (planform) at each cross section was then chosen to yield a smooth fairing between the original nose section and the outside of the inlet face. Comparison of faired forebody iterations 1 and 2 with the original is shown in Fig. 4. Thus, the first two iterations were modeled to demonstrate planform effects.

Horizontal survey plane perturbation velocity components for forebodies 1 and 2 are compared in Fig. 5 with those produced by the original forebody. The flow about the origi-

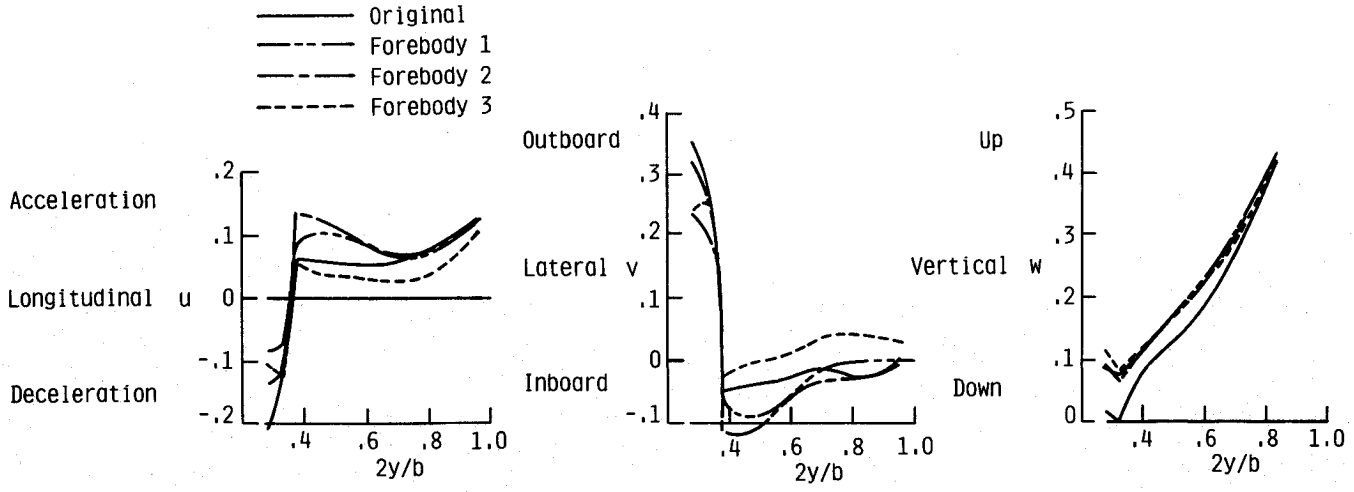


**Fig. 5 Comparison of horizontal survey plane perturbation velocities: Mach = 1.80, $\alpha$ = 9 deg.**

nal configuration is characterized by a longitudinal deceleration and lateral acceleration, i.e., a blockage effect near the fuselage, as would be expected. Outboard of about the 40% semispan location, the flow reaccelerates longitudinally and decelerates laterally. This reflects a sharply diminished fuselage effect and a corresponding straightening of the flow. The blockage effect is limited in its spanwise extent because of the supersonic freestream and the reduced forebody width ahead of the fuselage/wing junction. Faired forebody 1 produces considerably less longitudinal deceleration and lateral acceleration near the fuselage than does the original. Faired forebody 2 is an improvement in the velocity match in this region. Outboard of the 40% semispan the opposite is true; forebody 1 matches the velocities better than forebody 2. Both forebodies 1 and 2 produce considerably more upwash than does the original.

The effect of forebody profile was evaluated with forebody 3. Forebody 3 was modeled using the same planform and camber description as forebody 2. The profiles of forebodies 2 and 3 are also compared in Fig. 4. The effect of the forebody profile on the perturbation flowfield is included in the PAN AIR comparison of Fig. 5. Reducing forebody profile area resulted in a marked improvement in the perturbation velocity comparisons outboard of the 40% semispan location without much degradation of the inboard comparisons.

Further investigations of the effect of departing from the original camber or nose droop coupled with the knowledge of the effect of the gross distortions examined with forebodies 1-3 led to geometry iterations exemplified by forebodies 9 and 17. The geometries are compared in profile and camber with the original in Figure 6. In planform, forebodies 9 and 17 match that of forebody 2. In profile, both forebodies 9 and 17 represent compromises between the profiles examined with forebodies 2 and 3. Forebodies 9 and 17 reflect a slightly modified camber, shown in the figure, to reduce the upwash at the wing leading edge. The primary difference between forebodies 9 and 17 is in area distribution, as shown in Fig. 7. The area distribution of forebody 17 aft of the original inlet location was increased without a change in profile or planform by using superelliptical cross sections with an $\epsilon$ of 1.0. This also proved necessary to satisfy the contour constraint at the forebody/center fuselage splice station.

The horizontal plane perturbation velocities for forebodies 9 and 17 are shown in Fig. 8. Both forebodies produce similar velocity traces and reasonable comparisons with the original. When viewed in the vertical survey plane (Fig. 9) forebody 17 compares more favorably with the original velocity perturbations.

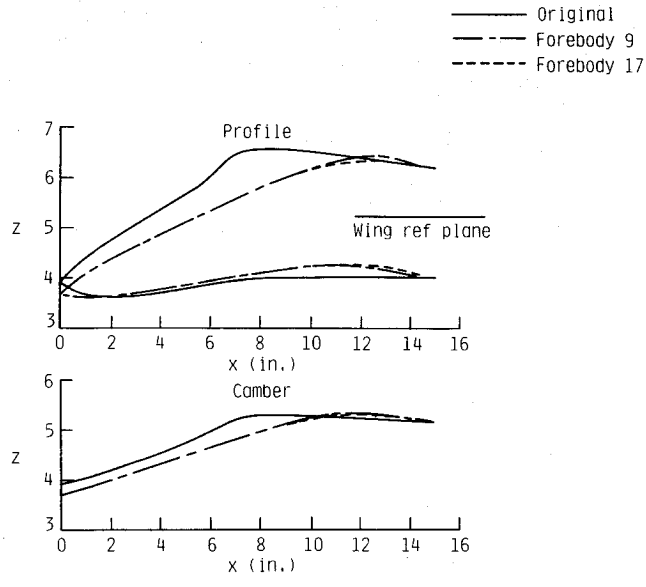


**Fig. 6 Profile and camber comparison.**

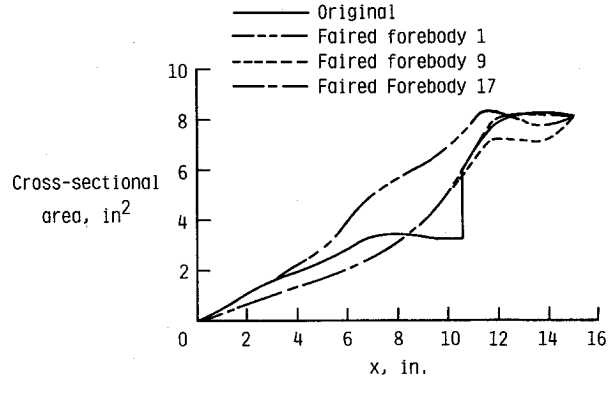


**Fig. 7 Area distribution comparisons.**

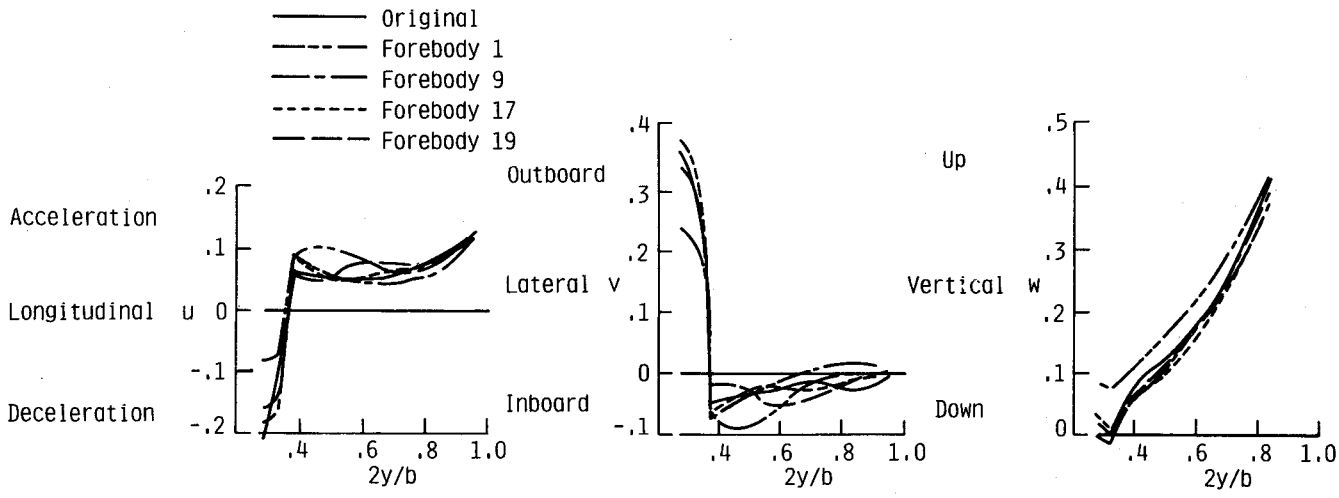


**Fig. 8 Comparison of horizontal survey plane perturbation velocities: Mach = 1.80, $\alpha$ = 9 deg.**

Although it did not produce an exact match in velocity perturbations, forebody 17 was deemed an acceptable representation of the original forebody, especially considering the manual iteration procedure and geometric constraints. Forebody 17 was the initial choice for hardware fabrication. In detailed model design, however, the need for further revision became necessary to improve the blending of the fuselage and wing. Forebody 19 represents the forebody that was fabricated and tested. The differences in forebodies 17 and 19 are in cross-sectional area only at stations aft of the fuselage/wing junction. (This was because of the aforementioned contour constraint.) Differences in the PAN AIR surveyed velocities that ensued are also shown in Figs. 8 and 9. In the horizontal survey plane, forebody 19 led to a general degradation in the velocity comparison, especially in the lateral component at 40% semispan. However, in the vertical survey plane, forebody 19 produced a slight improvement in the agreement with the baseline velocity survey. This comparison serves to show how sensitive the perturbation velocities in the selected survey planes are to changes in fuselage geometry.

After 19 iterations the development was stopped because the changes in the physical surface shape were becoming insignificant between iterations. Although the perturbation velocity match is not exact, the agreement in the regions near the wing leading edge is acceptable. The resulting equivalent faired forebody/model combination is pictured in Fig. 10. It should be noted that the solution obtained is not necessarily unique, as other "equivalent" forebody solutions could be possible depending on the initial analytical model selected.

In summary, the design approach consisted of gaging the effects of large geometric perturbations, i.e, profile, planform, and camber or droop, to an initial guess forebody, followed by fine adjustments to forebody camber and area distribution near the wing/fuselage junction. Some general observations are as follows:

1) As might be expected, changes in the perturbation velocities in the selected survey planes were most sensitive to fuselage contour changes in the immediate vicinity of the planes. Although not investigated, it is assumed that increasing forebody length would not have a great effect because of the distance of the nose-tip from the survey planes.

2) Forebody area distribution, determined mostly by profile since the forebody planform is constrained, and local surface slope play an important role in controlling the lateral and longitudinal perturbation velocities. Matching the flowfield of the original configuration requires dissipating the flow, originally captured by the inlets, about the fairing without excessive longitudinal deceleration or lateral acceleration.

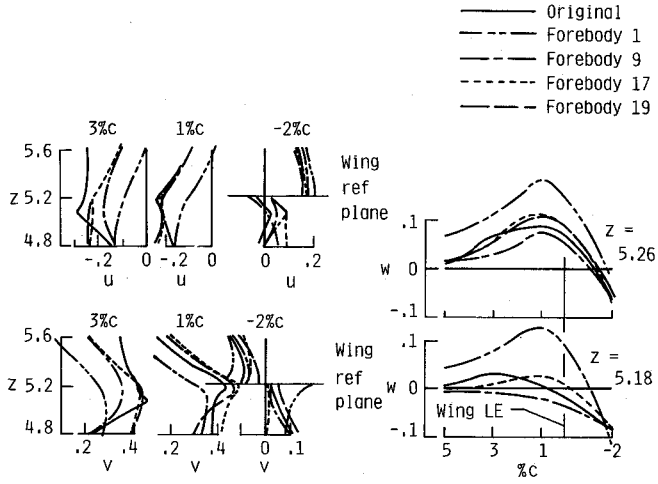


**Fig. 9 Comparison of vertical survey plane perturbation velocities: Mach = 1.80, $\alpha$ = 9 deg.**

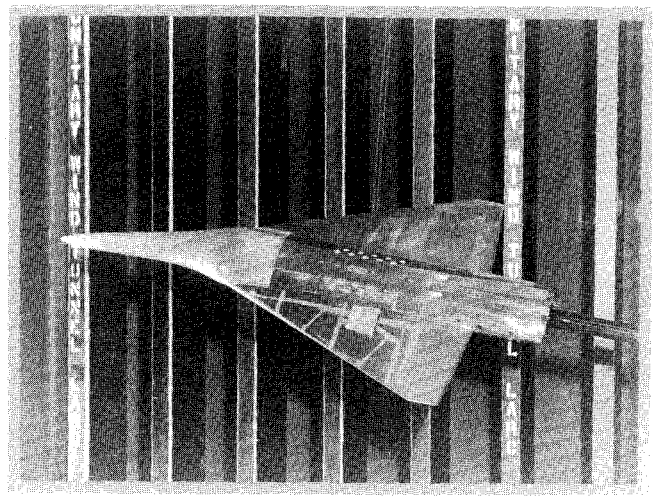

**Fig. 10 Equivalent configuration installation photograph.**

3) Lower surface contour near the wing leading edge plays an important role in controlling the upwash. However, modifying the nose droop proved to be the key to better matches in upwash.

4) A good initial equivalent forebody could be obtained by matching the camber and profile of the original forebody and then using a smooth fairing of the cross-sectional area distribution to determine the planform from the equation for the area of an ellipse.

**Wind-Tunnel Test**

The equivalent forebody wind-tunnel validation program was conducted in NASA Langley's Unitary facility.[4] The original and equivalent configurations were tested with a flat NACA 0005-82.5 airfoil section clipped delta wing, in addition to fuselage-alone tests. Each configuration was tested at Mach numbers of 1.6, 1.8, 2.0, and 2.16 at a Reynolds number of $2 \times 10^6$/ft. The model was installed on a sting-mounted six degree-of-freedom strain-gauge balance. The angle-of-attack range was $-4$ to 16 deg with sideslip angles of 0 and 5 deg.

The flat NACA 0005-82.5 airfoil was chosen, based on the computational results of Wood and Miller,[5] as a benchmark for future camber design efforts. The wing was pressure instrumented with the pressure line routings incorporated into a manifold system to allow easy disconnection for unobstructed force and moment testing. The pressure orifices were oriented in four spanwise rows; on the upper surface of the right wing and on the lower surface of the left wing. To insure boundary-layer transition, the wing had a 0.125-in. width of #60 grit located 0.2 in. perpendicular from the leading edge.[6] (All applicable model surfaces had grit at the appropriate locations.)

**Experimental Results**

*Force Data*

A force and moment comparison of the original and equivalent configurations, as well as the fuselage-alone configurations, are shown in Fig. 11 for Mach 1.8. The lift curves are concurrent at about 3 deg angle of attack and both exhibit a slight break from linearity at 10 deg angle of attack. The major aerodynamic difference between the two configurations is that the equivalent configuration has an average 0.0017 lower $C_D$ over the entire range of angle of attack. The pitching moment characteristics of the two configurations are very similar, the equivalent having a slightly negative moment shift. Since the aerodynamic performance was not considered in the design process of the equivalent forebody, it is not surprising that small differences exist in the force data. In fact, several factors can be identified that would affect the aerodynamic force results. The increased cross-sectional area and increased external wetted area of the faired forebody ahead of the inlet location would tend to cause an increase in wave drag and external skin friction drag, respectively. The elimination of the oblique inlet shocks would also tend to decrease drag. Probably the largest effect would be due to the elimination of all internal skin friction drag and the normal shocks contained in the inlet ducts of the original configuration. Since all of these effects are restricted to the fuselage, and since the design of the equivalent forebody sought to duplicate the forebody-induced perturbations on the wing flowfield, one would expect the aerodynamic force differences to originate from the forebody/fuselage alone. Comparison of the body-alone configurations is shown in Fig. 11 for the design Mach number. From the figure it can be seen that, indeed, the equivalent configuration has a drag-curve decrement of about 17 counts. These results were consistent throughout the test Mach number range.

*Flow Visualization*

Oil-flow photography seems to show that both the original and equivalent configurations develop a small region of leading-edge separation at angles of attack greater than 4–6 deg.

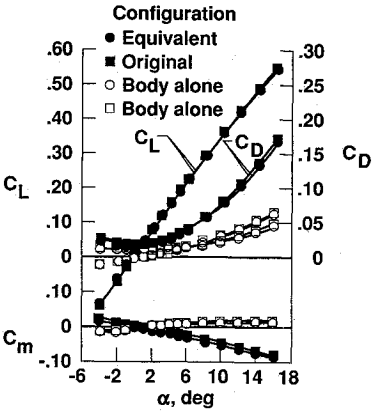


**Fig. 11 Force and moment comparison: Mach = 1.80.**

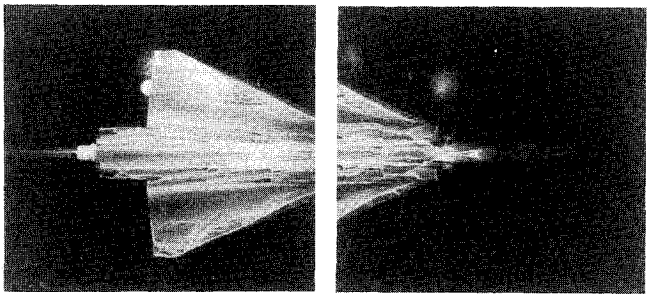

**a) Original configuration**

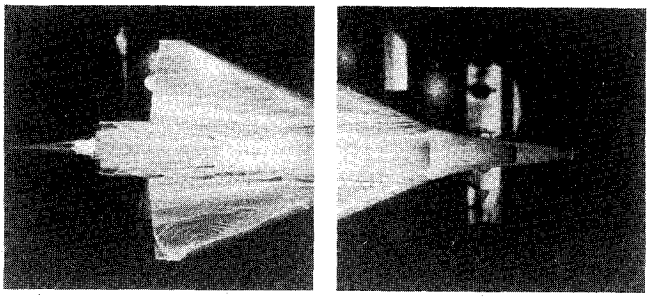

**b) Equivalent configuration**

**Fig. 12 Oil-flow photograph comparisons: Mach = 1.80, $\alpha$ = 8 deg.**

Figure 12 shows oil-flow photographs of the original and equivalent configurations at Mach 1.8 and angle of attack of 8 deg. (Because of the viewing restrictions in the wind-tunnel test section, two photographs are required to see the full configuration.) Oil accumulation lines are clearly visible just back from the leading edge of both configurations, indicating flow separation. Oil accumulation lines near the trailing edge of both configurations (particularly evident near the wing tips) suggest the onset of trailing-edge separation. No evidence of strong vortical activity over the wing was observed. Unfortunately, the schlieren and vapor-screen photographs that were obtained were not of a quality suitable for publication.

*Pressure Data*

Measured surface pressure results indicate that the equivalent-faired forebody simulates the effects of the original forebody on the wing flowfield to an acceptable degree of accu-

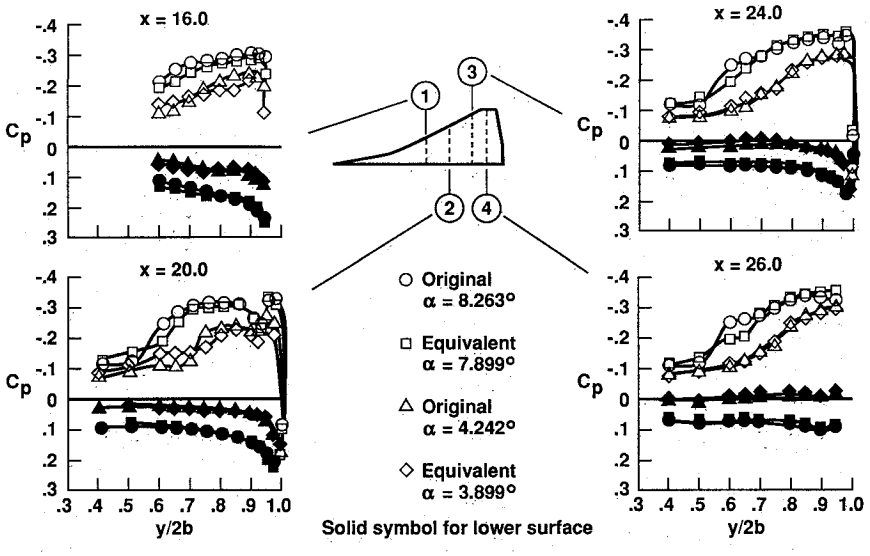


Fig. 13 Pressure coefficient comparisons: Mach = 1.80.

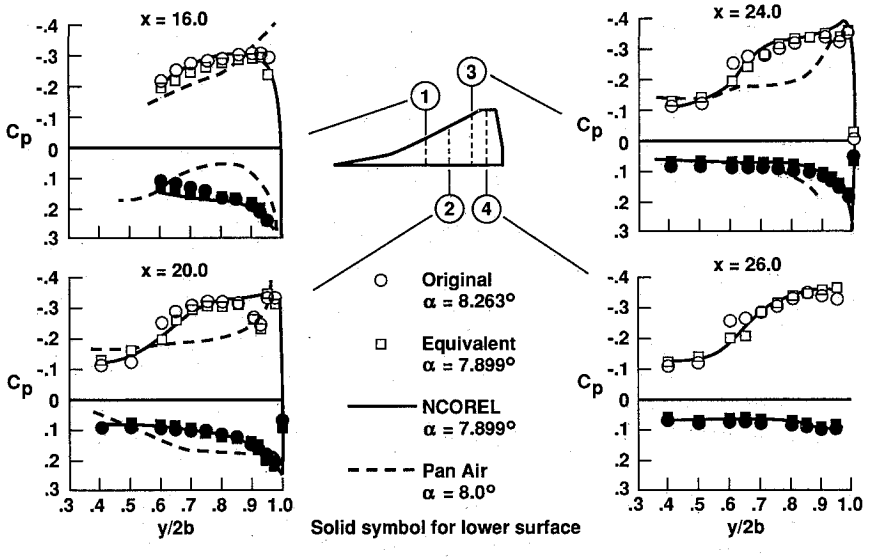


Fig. 14 Pressure coefficient computational comparisons: Mach = 1.80.

racy. Plots of wing pressure data at four model longitudinal locations for 4 and 8 deg angle of attack with Mach number of 1.8 are presented in Fig. 13 for both configurations. One should note that, for all pressure data comparisons, slight differences in the angle-of-attack data points exist between the equivalent and original configurations. This is owing to the experimental nature and need not be considered an adverse factor. (The difference generally being less than 0.5 deg.) The correlation of the pressure distributions on the lower surface is excellent for all the stations. At each station the original configuration pressures are slightly higher, but, considering the difference in angle of attack (the original configuration was at 0.4 deg higher angle of attack at this particular datum), this would be expected. At station 1, the upper-surface pressures are somewhat higher for the equivalent configuration. The differences are small around the leading edge, but, as the cross-flow shock area is approached, the equivalent configuration pressures are lower. At station 2 the upper-surface pressure differences are small around the leading edge, but the equivalent configuration pressures become significantly higher in the cross-flow shock region. The distributions at stations 3 and 4 are very similar, the only exception being around the leading edge of station 4 where the equivalent configuration pressures are somewhat lower. The differences around the leading edge of station 4 can most likely be attributed to slight differences in the area of trailing-edge separation between the two configurations as suggested by oil-flow and vapor-screen photography. Thus, the pressure data show that the primary flowfield irregularity between the two configurations is an outboard shift and slight weakening of the cross-flow shock for the equivalent configuration. This is believed to be because of the increased flow in the fuselage region that would have been captured by the inlets of the original configuration. It is interesting to note, considering the shift of the cross-flow shock, that the pressure correlation inboard of the shock is excellent.

A curious aspect of the pressure distributions of both configurations is a localized pressure spike located on the upper surface just inboard of the leading edge at stations 2 and 3. At station 2, the spike represents a $C_p$ increase of about 0.1 with the peak located at 92.5% semispan. At station 3, the spike is much weaker and is located at 97.5% semispan. These locations roughly correspond to the location of the oil accumulation lines noted in the oil-flow photographs of Fig. 12. Almost as interesting as the existence of the pressure spikes is their absence at stations 1 and 4. Referring again to the oil-flow photograph in Fig. 12, it can be seen that, in the area of station 1, the oil accumulation lines are dispersed. Likewise, in the aft area of station 4, the area of trailing-edge separation can be seen to encompass the leading edge at the tip, terminating the aforementioned accumulation line. Considering the observations of Kulfan and Sigalla[7] regarding leading-edge separation on rounded leading-edge delta wings, it can be shown that, for Mach 1.8, the configurations would tend to experience leading-edge separation for angles of attack greater than about 6 deg. Thus, it is believed that the anomalous pressure behavior is due to localized viscous effects (separation), as suggested by the oil-flow photographs.

While the differences in the pressure distributions are small at the design angle of attack, Fig. 13 reveals that the pressure distribution correlations degrade slightly at the lower angles of attack, at the design Mach number. Considering the possible differences in the wing flowfield between the two configurations, one would expect the largest differences to be restricted to the wing leading edge, primarily over the forward portions of the wing and attenuating with distance downstream. Referring again to Fig. 13, one can verify that, indeed, the greatest discrepancies in the pressure distributions generally occur at the most forward station: station 1.

### Computational Comparisons

Computational analyses were performed on the equivalent configuration with the PAN AIR code, used in the design, and NCOREL,[8] a full-potential method. Initially, the PAN AIR analysis was conducted to determine the applicability of using a linear panel method for such a design process. An NCOREL full-potential analysis was performed to examine the expected nonlinear effects arising from designing at such a relatively high $C_L$ for supersonic speeds. The computed drag values were adjusted to account for skin-friction drag by adding an empirical flat-plate skin-friction estimate[9] of $C_{Df} = 0.00679$ to the drag results obtained from the codes.

*PAN AIR Results*

A comparison of the PAN AIR predicted pressure coefficient distributions with the experimental data is shown in Fig. 14. In general, the PAN AIR code does a poor job of predicting the surface pressures at each of the first three stations. (PAN AIR data was not available for station 4.) The lower-surface pressure comparison is the better of the two, giving an adequate representation of the pressure trends. The upper surface does not represent pressure trends, and, in some cases, fails even to predict the $C_p$ magnitude to an acceptable degree of accuracy. This is especially true at station 3. The PAN AIR force predictions are much better than would be expected, considering the poor pressure predictions. A comparison is shown in Fig. 15 for the design Mach number.

The poor pressure coefficient predictions and yet fortuitous integrated force results seem to be a characteristic of linear codes when applied to high alpha, supersonic flows. Pittman et al.[10] have noticed similar linear code performance in a supersonic, attached-flow, high-lift design. In fact, in view of the rather poor PAN AIR pressure predictions, it seems fortunate that the equivalent forebody matched the perturbations of the original forebody as well as it did.

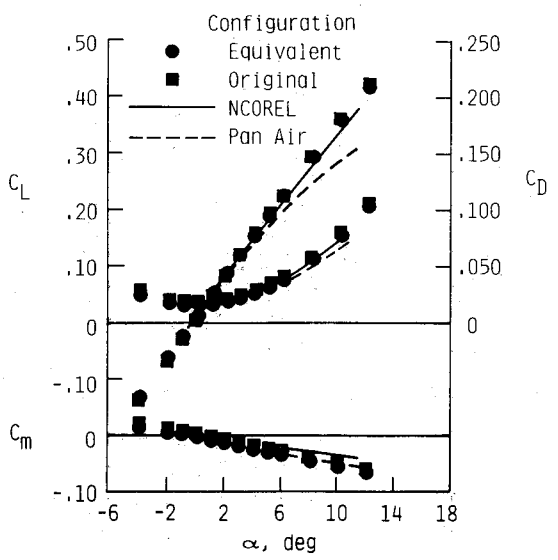


**Fig. 15 Force and moment computational comparisons: Mach = 1.80.**

*NCOREL Results*

The NCOREL code is a supersonic marching scheme based on the full-potential method with a bow-shock entropy correction. Pressure data were interpolated at each of the model stations from a mesh size of $29 \times 29$ and a step size of 1.0 in. A comparison of the NCOREL predicted pressure coefficient distributions with the experimental data is also shown in Fig. 14 for the equivalent configuration at an angle of attack of 7.9 deg at Mach 1.8. At station 1, minor differences exist inboard of about 75% semispan. The predictions and test data at stations 2 and 3 correlate well on the lower surface, around the leading edge, and in the cross-flow recompression region. However, NCOREL does not predict the observed pressure spikes located at 90–95% semispan. Regarding these unusual pressure data, similar pressure phenomena has been observed by Pittman[11] for a cambered delta wing at Mach 1.62. However, in that case the observed pressure spikes were the result of leading edge surface tailoring and were accurately predicted by the NCOREL code. Thus, if the unusual pressure data were the result of nonviscous effects, the NCOREL code should have accurately predicted that behavior. Correlation at the last station 4, is good on the lower surface, but degrades around the leading edge and on the upper surface. This is most likely the result of trailing-edge separation as indicated in the vapor-screen photographs.

Plots of the NCOREL force predictions are also shown in Fig. 15. The code accurately predicts the $C_L$ and inviscid $C_D$ up to angles of attack of about 10 deg, but errors exist in the pitching-moment prediction, most likely due to incorrect modeling of the fuselage aft of the wing (the computational models were cut off at the wing trailing edge). The trailing edge itself has a slight forward sweep but was modeled with no sweep to reduce complexity.

## Conclusions

In the design of the equivalent-faired forebody to replace a forebody with flowing inlets, the fundamental requirement of velocity flowfield matching in the region of the survey planes results in matching of the surface pressure distributions on the wing. The results show adequate pressure field matching over several stations on the wing with the most notable difference being an outward shift and slight weakening of the cross-flow shock for the equivalent configuration. This is most likely due to the additional flow around the fuselage that would have been captured by the inlets of the original configuration.

While aerodynamic performance factors were not addressed in the design of the equivalent forebody, the force and mo-

ment differences between the two configurations are minor except for the reduced drag of the equivalent configuration primarily due to the elimination of internal duct losses. Also, weak oblique shock systems, visible in schlieren and vapor-screen photographs emanating from the canopy and inlets of the original forebody, probably contribute somewhat to the higher drag levels of the original configuration.

Areas of localized leading-edge separation, indicated by surface pressure and flow-visualization data, are virtually identical on both the original and equivalent configurations. Since separation is a critical concern in the design of supersonic wings at high lift coefficients, the identical leading-edge separation indications between the two configurations demonstrate the applicability of using the equivalent forebody approach in preliminary wing design studies. Thus, a simple equivalent-faired forebody can be used to simulate realistic flowfield perturbations like those produced by a complex forebody with inlets.

Comparison of the computational analyses with the experimental data indicates that, for the design conditions considered here, the flowfield is apparently significantly nonlinear. Thus, the applicability of linear theory methods within the flight regime of moderate supersonic Mach number and high angle of attack is questionable. However, nonlinear full-potential methods do a good job of modeling the wing-body flowfield.

In summary, the flowfield of the equivalent-faired forebody matches the flowfield of a much more complex forebody with flow-through inlets to an acceptable degree for baseline experimental and computational research. The faired forebody greatly reduces computational and experimental complexity, and substantially reduces model design and fabrication costs.

## References

[1]O'Neill, P. J. and Verhoff, A., "The Equivalent Simple Body (ESB) Method for Transonic Wing Analysis," *Proceedings of the AIAA/ASME 3rd Joint Thermophysics, Fluids, Plasma, and Heat Transfer Conference,* AIAA, New York, 1982.

[2]Sidwell, K. W., Baruah, P. K., and Bussoletti, J. E., "PAN AIR Volume II – User's Manual," Version 1.0, NASA CR-3252, May 1980.

[3]Wood, R. M. and Miller, D. S., "Wing Planform Effects at Supersonic Speeds for an Advanced Fighter Configuration," NASA TP-1905, 1981.

[4]Jackson, C. M., Jr., Corlett, W. A., and Monta, W. J., "Description and Calibration of the Langley Unitary Plan Wind Tunnel," NASA TP-1905, 1981.

[5]Wood, R. M. and Miller, D. S., "Impact of Airfoil Profile on the Supersonic Aerodynamics of Delta Wings," AIAA Paper 85-4073, Oct. 1985.

[6]Braslow, A. L., Hicks, R. M., and Harris, R. V., Jr., "Use of Grit-Type Boundary-Layer Transition Trips on Wind-Tunnel Models," NASA SP-124, 1966; (also available as NASA TN D-3579).

[7]Kulfan, R. M. and Sigalla, A., "Real Flow Limitations in Supersonic Airplane Design," AIAA Paper 78-147, Jan. 1978.

[8]Siclari, M. J., "An Improved Version of NCOREL," NASA CR-4165, 1988.

[9]Sommer, S. C. and Short, B. J., "Free-Flight Measurements of Turbulent-Boundary-Layer Skin Friction in the Presence of Severe Aerodynamic Heating at Mach Numbers from 2.8 to 7.0," NASA TN-3391, 1955.

[10]Pittman, J. L., Miller, D. S., and Mason, W. H., "Supersonic, Nonlinear, Attached-Flow Wing Design for High Lift With Experimental Validation," NASA TP-2336, 1984.

[11]Pittman, J. L., "Experimental Flowfield Visualization of a High Alpha Wing at Mach 1.62," *Journal of Aircraft,* Vol. 24, May 1987, pp. 335–341.